A Strict Framework for Analyzing Linear and Nonlinear Propagation in Photonic and Terahertz Graphene Waveguides

Alexandros Pitilakis, Dimitrios Chatzidimitriou, and Emmanouil E. Kriezis, *Senior Member, IEEE*
Aristotle University of Thessaloniki, Department of Electrical and Computer Engineering,
Division of Telecommunications, Thessaloniki, GR-54124, Greece
Tel: (+30) 2310 99 6362, Fax: (+30) 2310 99 6312, e-mail: alexpiti@auth.gr

ABSTRACT
Two-dimensional (sheet) materials, with graphene being a prominent example, are recently finding their way in a variety of photonic and terahertz waveguide applications. We provide a framework for the rigorous study of three-dimensional guided-wave devices that comprise both bulk and sheet materials. Our formulation, relying on the finite element method, allows for arbitrary anisotropy in the susceptibility and surface conductivity tensors describing bulk and sheet material properties, respectively. A number of emerging graphene-comprising waveguide platforms are critically assessed, targeting both linear and in particular nonlinear (third-order) applications in the near- and far-infrared spectral region.
Keywords: graphene, waveguides, nonlinear propagation, photonic circuits, plasmonics, terahertz.

1. INTRODUCTION

Graphene, a two-dimensional sheet of hexagonally-arranged carbon atoms, is without doubt one of the most promising new materials, finding its way into diverse research fields including nanotechnology, photonics and plasmonics [1]. One of the most interesting properties of graphene is the ability to control its conductivity by shifting its Fermi level, via externally applied bias-voltage and at fabrication via doping [2]-[4]. This has been exploited to demonstrate a number of applications like modulators, photodetectors and polarizers [4].

This work focuses on graphene-comprising waveguides and their applications, with emphasis on nonlinear propagation, in the optical and Terahertz (THz) band. Firstly, we will present a full-vector electromagnetic-modelling formulation, able to handle inhomogeneous three-dimensional structures comprised of both sheet (2D) and bulk (3D) materials, in the spectral domain. Our model properly accounts for anisotropy in the complex-valued susceptibility and conductivity tensors describing bulk and sheet material properties, respectively. Subsequently, using a finite element method (FEM) implementation in conjunction with graphene parameters from available theoretical models, we will study linear and nonlinear propagation properties in various photonic, plasmonic and THz waveguides, identifying optimized configurations and highlighting interesting prospects.

2. ELECTROMAGNETIC MODELING

Electrically conductive materials generate a current density that modifies Maxwell's curl equations, as expressed in the frequency domain and derived under the $\exp(-i\omega t)$ sign convention,

$$\nabla \times \tilde{\mathbf{E}} = +i\omega\mu_0\overline{\mu}_r\tilde{\mathbf{H}}, \tag{1}$$

$$\nabla \times \tilde{\mathbf{H}} = -i\omega\left(\varepsilon_0\tilde{\mathbf{E}} + \tilde{\mathbf{P}}\right) + \tilde{\mathbf{J}}, \tag{2}$$

where $\tilde{\mathbf{P}} \propto \varepsilon_0\chi\tilde{\mathbf{E}}$ is the electric polarization and $\tilde{\mathbf{J}} \propto \sigma\tilde{\mathbf{E}}$ is the electric current density, according to Ohm's law. The bar (e.g. in $\overline{\mu}_r$) denotes a tensor in $\mathbb{R}^3$, describing material properties and having an instantaneous response. Both $\mathbf{P}$ and $\mathbf{J}$ can be expressed as tensor-product power-series in the time-domain electric-fields,

$$\mathbf{P} = \varepsilon_0\overline{\chi}^{(1)} \mid \mathbf{E} + \varepsilon_0\overline{\chi}^{(2)} \mid \mathbf{EE} + \varepsilon_0\overline{\chi}^{(3)} \mid \mathbf{EEE} + \ldots, \tag{3}$$

$$\mathbf{J} = \left[\overline{\sigma}_b^{(1)} + \overline{\sigma}_s^{(1)}\delta_s\right] \mid \mathbf{E} + \left[\overline{\sigma}_b^{(2)} + \overline{\sigma}_s^{(2)}\delta_s\right] \mid \mathbf{EE} + \left[\overline{\sigma}_b^{(3)} + \overline{\sigma}_s^{(3)}\delta_s\right] \mid \mathbf{EEE} + \ldots, \tag{4}$$

where $\overline{\chi}^{(n)}$ and $\overline{\sigma}_b^{(n)}$ are (n+1)-rank bulk-susceptibility and bulk-conductivity tensors, respectively, $\overline{\sigma}_s^{(n)}$ is the (n+1)-rank surface-conductivity tensor measured in [S(m/V)$^{n-1}$] and δ_s (in units of m^{-1}) is a surface-Dirac function defined on the conductive sheet. The first term in equations (3) and (4) corresponds to linear response and the following ones to nonlinear response; in this work we only consider the third-order nonlinear response. In equation (4), the electric current density is made of bulk and sheet contributions, $\mathbf{J} = \mathbf{J}_b + \mathbf{J}_s\delta_s$. However, bulk conductivity can be introduced as an imaginary part to the susceptibility tensor of respective rank, so that we can replace $\tilde{\mathbf{P}} \to \tilde{\mathbf{P}} - \tilde{\mathbf{J}}_b / (i\omega)$ and $\tilde{\mathbf{J}} \to \tilde{\mathbf{J}}_s\delta_s$ in (2). In this case, and in the absence of sheet materials, $\tilde{\mathbf{J}}$ vanishes from equation (2), simplifying the formulation. In all other cases, the surface conductivity tensors $\overline{\sigma}_s^{(n)}$ have to be taken into account. The resulting surface current perturbs the continuity of the tangential components of the magnetic fields across the faces of the sheet according to the boundary condition $\mathbf{n} \times (\tilde{\mathbf{H}}_2 - \tilde{\mathbf{H}}_1) = \tilde{\mathbf{J}}_s$, where $\mathbf{n}$ is the unit vector normal to the sheet, with direction from bulk medium 1 to medium 2.

Sheet materials are implicitly anisotropic in vectorial $\mathbb{R}^3$ formulations. Specifically, the surface current $\tilde{\mathbf{J}}_s$ in graphene can only have components tangential to the sheet. The second-rank surface conductivity tensor of a "reference" sheet (infinite, homogeneous, planar and normal to the y-axis) can be generically expressed as

$$\bar{\sigma}_s^{(1)} = \begin{bmatrix} \sigma_{s,xx} & 0 & \sigma_{s,xz} \\ 0 & 0 & 0 \\ \sigma_{s,zx} & 0 & \sigma_{s,zz} \end{bmatrix}, \tag{5}$$

containing up to four independent complex-valued parameters. However, for most practical applications, graphene exhibits a number of symmetries, namely $\sigma_{s,xx} \equiv \sigma_{s,zz} = \sigma_c$ and $\sigma_{s,xz} = \sigma_{s,zx} = 0$, so that it can eventually be modelled by a single surface conductivity complex value (σ_c, in Siemens), apart from the normal vector ($\mathbf{n}$). In this simple case, the linear surface current can be expressed as

$$\tilde{\mathbf{J}}_s = \bar{\sigma}_s^{(1)}\tilde{\mathbf{E}} = \sigma_c \tilde{\mathbf{E}}_{\|} = \sigma_c \left[\mathbf{n} \times (\tilde{\mathbf{E}} \times \mathbf{n})\right], \tag{6}$$

where $\tilde{\mathbf{E}}_{\|}$ is the tangential to the sheet E-field component. For inhomogeneous (or non-planar) sheets, the value of σ_c (or $\mathbf{n}$) can vary in space. Finally, when $\mathbf{n}$ has a non-trivial orientation [unlike $\mathbf{n} \equiv \mathbf{y}$ in equation (5)], all nine elements of $\bar{\sigma}_s^{(1)}$ can be nonzero, and are acquired with a rotation of the "reference" tensor.

Similar simplifications apply also for the fourth-rank nonlinear surface conductivity tensor, $\bar{\sigma}_s^{(3)}$, and the resulting nonlinear surface current, $\tilde{\mathbf{J}}_{s,\mathrm{NL}}$. Specifically, assuming the simplest model of graphene nonlinearity [5]-[6], the $jklm$-th element of $\bar{\sigma}_s^{(3)}$ is given by

$$\sigma_{s,jklm}^{(3)} = \sigma_3 \frac{1}{3}\left(\delta_{jk}\delta_{lm} + \delta_{jm}\delta_{kl} + \delta_{jl}\delta_{mk}\right), \tag{7}$$

where δ_{pq} is the Kronecker delta, σ_3 is the single complex-valued nonlinear surface conductivity and indices $\{j,k,l,m\}$ scan the two Cartesian components tangential to the sheet. This amounts to 8 nonzero elements in $\bar{\sigma}_s^{(3)}$, out of the 81 in total. In the most general case up to 14 nonzero elements (6 independent) are allowed in graphene $\bar{\sigma}_s^{(3)}$, while still satisfying the condition $\tilde{\mathbf{J}}_{s,\mathrm{NL}} \cdot \mathbf{n} = 0$ [6]. Similarly to $\bar{\sigma}_s^{(1)}$, when the graphene sheet is not normal to a principal axis, $\bar{\sigma}_s^{(3)}$ is acquired with a rotation of the reference tensor.

2.1 Equivalent Bulk Medium Approximation

Sheet media can be approximated by "equivalent" bulk-media layers [3] of nonzero thickness d (in the case of graphene, d=0.34 nm). The equivalent susceptibility tensors are given by $\bar{\chi}_{\mathrm{eq}}^{(n)} = i\sigma_s^{(n)} / (\omega\varepsilon_0 d)$, where $\bar{\sigma}_s^{(n)}$ are the surface conductivity tensors of respective rank; thus, any anisotropy in $\bar{\sigma}_s^{(n)}$ is directly inherited by the equivalent bulk susceptibility. Using the simplest expressions of linear and nonlinear surface conductivity tensors of equations (6) and (7), the fundamental complex-valued parameters of the equivalent bulk medium are given by $\varepsilon_{r,\mathrm{eq}} = 1 + \chi_{\mathrm{eq}}^{(1)}$ and $n_{2,\mathrm{eq}} = 3\chi_{\mathrm{eq}}^{(3)} Z_0 / (4\varepsilon_{r,\mathrm{eq}})$, respectively, where $\chi_{\mathrm{eq}}^{(1)} = i\sigma_c / (\omega\varepsilon_0 d)$ and $\chi_{\mathrm{eq}}^{(3)} = i\sigma_3 / (\omega\varepsilon_0 d)$. This equivalent representation is useful in case a numerical implementation allowing only bulk-media needs to be utilized. However, we stress that comparison of bulk medium properties (e.g. n_2) with the equivalent properties of sheet media (e.g. $n_{2,\mathrm{eq}}$) is often inapt and can lead to serious misconceptions.

2.2 Nonlinear Propagation Parameters

Using a perturbation on the linear eigenmode analysis of a waveguide [7]-[8], we can extract its complex-valued nonlinear parameter, γ_{NL} measured in [m^{-1}W^{-1}], which effectively controls the nonlinear phase-shift and losses of a high-power signal propagating along the waveguide [9]. Without going into details, it can be shown that $\gamma_{\mathrm{NL}} = \gamma_b + \gamma_s$, i.e. it comprises a bulk and sheet contribution, from respective material nonlinearities. The two contributions are calculated using an overlap integral over the entire cross-section of the waveguide ($\iint_S \mathrm{d}S$) and along the trace of the sheet on the cross-section ($\int_c \mathrm{d}\ell$), respectively, according to

$$\gamma_b = \frac{3\omega\varepsilon_0}{4(2\mathcal{N})^2} \sum_{jklm}^{xyz} \iint_S \chi_{jklm}^{(3)} e_j e_k^* e_l e_m^* \mathrm{d}S, \qquad \gamma_s = i\frac{3}{4(2\mathcal{N})^2} \sum_{jklm}^{xyz} \int_c \sigma_{s,jklm}^{(3)} e_j e_k^* e_l e_m^* \mathrm{d}\ell. \tag{8}$$

In these expressions, $\mathcal{N} = 0.5 \left| \iint (\mathbf{e} \times \mathbf{h}^*) \cdot \mathbf{z} \mathrm{d}S \right|$ is a normalization constant measured in Watts and $\mathbf{e}(x,y)$ is the cross-section profile of the eigenmode, both calculated from the linear problem. From equations (8), it can be inferred that the imaginary and real part of $\bar{\sigma}_s^{(3)}$ are responsible for nonlinear phase-shift and losses, respectively, which can in turn be related to the Kerr effect and two-photon absorption (TPA) in the waveguide.

3. APPLICATIONS

In terms of a FEM implementation of the formulation presented, graphene sheets are defined geometrically by surfaces/faces (i.e. by normal vector sets) and electromagnetically by reference surface conductivity tensors $\bar{\sigma}_{s,\mathrm{ref}}^{(1)}$ and $\bar{\sigma}_{s,\mathrm{ref}}^{(3)}$, which are attributed to each of the surfaces/faces of the geometry. Referring to the simplified

versions of equations (5) and (7), the complex values of the parameters σ_c and σ_3 are derived from closed-form expressions [2],[5] and typically depend on: wavelength, temperature, relaxation times and, most importantly, on the Fermi-level, here referred to as chemical potential, μ_c.

3.1 Optical Absorption Modulation

One of the simplest applications of graphene-comprising waveguides is the optical absorption modulator [4]. Tuning the μ_c of a graphene sheet via a bias voltage tunes its surface conductivity and thus tunes the guided mode's propagation losses, $\alpha = 1/L_{\text{prop}} = 2k_0 / \text{Im}\{n_{\text{eff}}\}$, where n_{eff} is the effective mode index. The performance metric of such an absorption modulator is the difference of propagation losses between the high- and low-loss regimes, $\Delta\alpha$. For graphene, the high-loss regime is for $\mu_c < \hbar\omega/2$, which signifies the onset of the interband absorption mechanism [2], whereas for $\mu_c > \hbar\omega/2$ graphene is practically transparent.

It has been experimentally demonstrated [4] that a silicon-wire waveguide overlaid with a graphene-alumina-graphene (GAG) cover, Fig. 1(a), can provide $\Delta\alpha$=0.16 dB/μm, which translates to 6 dB modulation depth for a 40 μm-long waveguide, in the λ=1.55 μm band. In this configuration, a parallel-plate capacitor is formed between the two graphene sheets separated by the thin Al_2O_3 (alumina) layer. Applying a voltage induces an approximately equal carrier (electron and hole) density on the two graphene sheets. If the sheets are assumed undoped, this leads to $\mu_{c,1} = -\mu_{c,2}$ for the two sheets which, in turn, translates to an equal surface conductivity σ_c due to graphene's band-structure symmetry [2]. The shift in the chemical potential as a function of applied voltage can be approximated by $\Delta\mu_c = \pm\hbar v_F(\pi\eta V_{\text{bias}})^{0.5}$, where $v_F = c_0/300$ is the Fermi velocity and $\eta = \varepsilon_0\varepsilon_d/(e\,t_d)$ is a parameter extracted from the parallel-plate capacitor model, assuming a dielectric of low-frequency dielectric constant ε_d and thickness t_d. In the case of [4], η=9×10^{16} /(m^{2}V) which means that the critical value μ_c=0.4 eV is attained for V_{bias}≈1.4 V.

Based on this configuration, we designed a waveguide comprising a planar GAG stack, Fig. 1(b), which is simpler to design and outperforms the design of [4]. The 7 nm-thick GAG stack is placed on top of a 50 nm-thick Si-slab and a 170 nm-thick by 300 nm-wide Si-wire is built on top of that. Keeping in mind that the GAG stack is a small perturbation, the E-field of the TE mode of this Si-rib waveguide optimally overlaps with the graphene sheets, fully exploiting the change in their σ_c. As presented in Fig. 1(c), our numerical FEM simulations revealed that a modulation depth $\Delta\alpha$>0.4 dB/μm can be attained with our waveguide design, whereas the design of [4] is theoretically limited to $\Delta\alpha$<0.25 dB/μm. Finally, we note that these waveguides can also be used as voltage-controlled phase modulator when μ_c is toggled between 0.4 eV (V_{bias}~1.4 V) and over 0.7 eV (V_{bias}>4 V); given this V_{bias} range, the calculated change in $\text{Re}\{n_{\text{eff}}\}$, Fig. 1(d), corresponds to a dephasing length of $L_\pi = 0.5\lambda/\Delta n_{\text{eff}}$~45 μm and 77 μm, for our waveguide and that of [4], respectively.

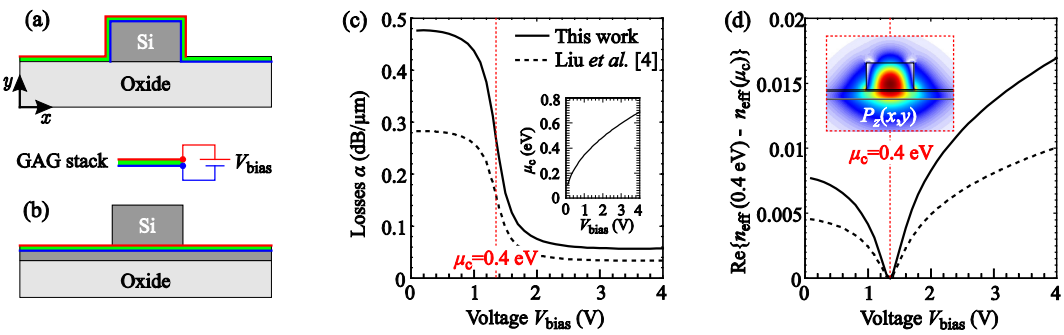

Figure 1. Cross-section of (a) reference [4] and (b) proposed waveguide designs, both containing a graphene-alumina-graphene (GAG) stack. (c) Propagation losses vs. voltage; inset: chemical potential vs. voltage. (d) Effective index change vs. voltage; inset: guided power density of proposed waveguide TE mode.

3.2 Nonlinear Propagation

In order to quantify the contribution of graphene's nonlinear surface-conductivity to the nonlinear parameter, we study hybrid and plasmonic optical waveguides, as well as graphene nanoribbons (GNR) in the THz regime.

Firstly, we consider a hybrid-plasmonic waveguide [8], namely a 200 nm-wide by 340 nm-high silicon-wire coated with PMMA and covered by an infinite graphene sheet with a 50 nm-thick silver film evaporated on top of it; the Si-wire is separated from the graphene/silver stack by a thin PMMA gap. This waveguide supports a TM mode, highly confined in the PMMA gap between the silicon and the metal. Despite its high confinement, the E-field of this mode is predominantly normal to the graphene sheet and thus it negligibly contributes to the nonlinear parameter. As can be seen in Fig. 2(a), bulk silicon nonlinearity (n_2 = 2.5×10^{-18} m^2/W) eventually dominates graphene/sheet nonlinearity, assuming σ_3=-i7.2×10^{-23} S(m/V)^2 [5]. Invoking the six extra "anisotropic" elements of $\bar{\sigma}_s^{(3)}$, i.e. $\tilde{s}$=1 in equation (13) of [6], leads to an improvement of two orders of

magnitude in the nonlinear parameter, dotted curve in Fig. 2(a), as these extra elements interact with the normal E-field.

Subsequently, we study a planar plasmonic waveguide made of a nanosized slot etched on a 20 nm-thick silver film evaporated on an oxide substrate, with the whole structure covered by an infinite graphene sheet. This waveguide supports a TE-polarized mode that is highly confined inside the metal-slot. This configuration provides an exceedingly high nonlinear parameter as the slot width decreases, Fig. 2(b). However, the mode losses also increase, dominated by the silver's bulk conductivity. Adding more graphene sheets increases both γ_s and α, meaning that the overall figure-of-merit $\mathcal{F} = \gamma / \alpha$ [8] is only slightly affected.

Finally, we consider an air-suspended 1 μm-wide GNR waveguide, operating at 10 THz, Fig. 1(c). This structure supports a plasmonic anti-symmetric TM-mode [10] with very high confinement at the edges of the ribbon, that leads to an exceedingly high γ_s and a propagation length in the order of 10λ. This result, along with the ability to tune both $\overline{\sigma}_s^{(1)}$ and $\overline{\sigma}_s^{(3)}$ via electric gating, suggests interesting THz applications using GNRs.

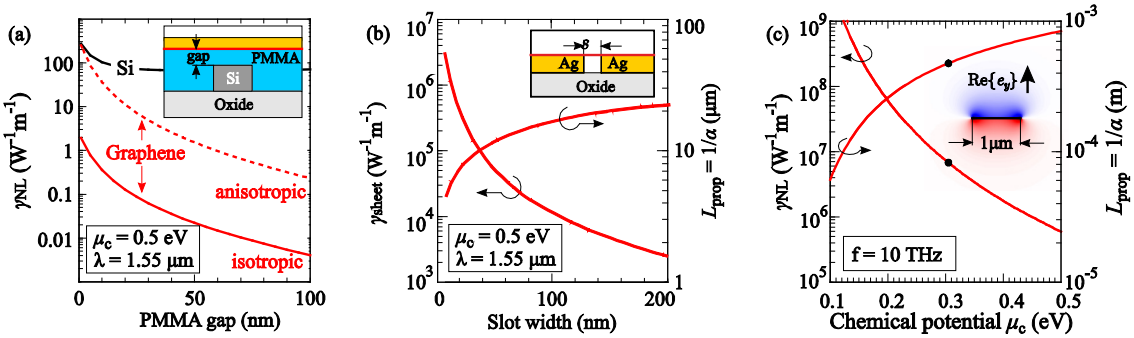

Figure 2. Graphene-comprising nonlinear waveguides: (a) Hybrid silicon-plasmonic, (b) Plasmonic metal-slot, (c) Air-suspended graphene nanoribbon supporting a plasmonic anti-symmetric TM mode at the THz regime.

4. CONCLUSIONS

We have presented a rigorous formulation for the numerical modelling of arbitrary three dimensional graphene-comprising waveguides. Our formulation is fully vectorial and allows for any anisotropy in the electric susceptibility and surface conductivity tensors, for bulk and sheet materials, respectively. We considered photonic and plasmonic optical waveguide designs and extracted their linear and nonlinear properties. Finally, we investigated the potential of tunable nonlinear graphene nanoribbons for applications in the THz regime.

ACKNOWLEDGEMENTS

Alexandros Pitilakis acknowledges the support of the "IKY Fellowships of Excellence for Postgraduate Studies in Greece – Siemens Programme". This research has been co-financed by the European Union (European Social Fund – ESF) and Greek national funds through the Operational Program "Education and Lifelong Learning" of the National Strategic Reference Framework (NSRF). Research Funding Program: THALES (Project ANEMOS). Investing in knowledge society through the European Social Fund.

REFERENCES

[1] K.S. Novoselov *et al.*: A roadmap for graphene, *Nature*, vol. 490 pp. 192-200, 2012.
[2] L.A. Falkovsky, Optical properties of graphene and IV-VI semiconductors, *Phys. Usp.*, vol. 178 pp. 923, 2008.
[3] A. Vakil and N. Engheta:"Transformation optics using graphene, *Science*, vol. 332 pp. 1291-1294, 2011.
[4] M. Liu, X. Yin, and X. Zhang: Double-layer graphene optical modulator, *Nano Lett.*, vol. 12 pp. 1482-1485, 2012.
[5] E. Hendry, P.J. Hale, J. Moger, A. K. Savchenko, and S.A. Mikhailov: Coherent nonlinear optical response of graphene, *Phys. Rev. Lett.*, vol. 105 pp. 97401, 2010.
[6] A. V. Gorbach, A. Marini, and D. Skryabin: Graphene-clad tapered fiber: Effective nonlinearity and propagation losses, *Opt. Lett.,* vol. 38 pp. 5244-5247, 2013.
[7] S. Afshar Vahid and T.M. Monro: A full vectorial model for pulse propagation in emerging waveguides with subwavelength structures part I: Kerr nonlinearity, *Opt. Express*, vol. 17 pp. 2298-2318, 2009.
[8] A. Pitilakis and E.E. Kriezis: Highly nonlinear hybrid silicon-plasmonic waveguides: Analysis and optimization, *J. Opt. Soc. Am. B*, vol. 30 pp. 1954-1965, 2013.
[9] T. Gu *et al.*: Regenerative oscillation and four-wave mixing in graphene optoelectronics, *Nat. Phot.*, vol. 6 pp. 554-559, 2012.
[10] A.Y. Nikitin, F. Guinea, F.J. Garcia-Vidal, and L. Martin-Moreno: Edge and waveguide terahertz surface plasmon modes in graphene microribbons, *Phys. Rev. B*, vol. 84 pp. 161407, 2011.